Journal of Applied Electrochemistry **32**: 551–559, 2002.

An MHD-based treatment of electrolysis in magnetic fields generated inside a solenoid

T.Z. FAHIDY
Department of Chemical Engineering, University of Waterloo, Waterloo ON N2L 3G1, Canada (e-mail: tfahidy@engmail.uwaterloo.ca)

Received 22 May 2002; accepted in revised form 23 May 2002

Key words: magnetoelectrolysis, magnetohydrodynamics, mass transport, solenoid, vorticity

Abstract

The effect of magnetic field superposition on electrolysis carried out in magnetic fields generated inside a solenoid is analysed using the theory of magnetohydrodynamics. It is shown that induced field inhomogeneity is responsible for the creation of local vortex motion which enhances ionic mass transport rates. A detailed vorticity analysis of two laboratory-scale, and a pilot plant-scale experimental magnetoelectrolytic cell serves for illustration.

List of symbols

a	mean solenoid radius (cm)
b	search point location on the solenoid axis (cm); electrode separation distance (cm) in Equations 18–23
$\boldsymbol{B}$	magnetic flux density (magnetic induction) vector (mT)
c	electrolyte concentration (mol dm^{-3})
c_e	cation concentration at the electrode surface (mol dm^{-3})
c_I	ionic concentration (mol dm^{-3})
c^*	dimensionless concentration
c_∞	cation concentration in the bulk (mol dm^{-3})
D	electrolyte diffusivity (cm^2 s^{-1})
D_i	ionic diffusivity (cm^2 s^{-1})
$\boldsymbol{e}$	unit vector
F	faradaic constant (96 487 C mol^{-1})
$F(a,b)$	geometric factor relationship defined by Equation 3(b)
$\boldsymbol{F}_T$	total external force vector (N)
h	height of the electrolyte level in the electrolytic cell (cm)
i_B	cathodic limiting current density in a magnetic field (A dm^{-2})
$i_{B=0}$	cathodic limiting current density in the absence of a magnetic field (A dm^{-2})
I	electric current (A)
$\boldsymbol{j}$	electric current density vector (A cm^{-2}); j_0 its magnitude
k_1	$I/2\pi\rho L_c$ (A cm^{-2} g^{-1}) (Equation 11)
k_2	k_1/v (C g^{-1}) (Equation 12)
$(k_M)_B$	mass transport coefficient in a magnetic field (cm s^{-1})
$(k_M)_{B=0}$	mass transport coefficient in the absence of a magnetic field (cm s^{-1})
K	proportionality factor between v_x and $x^{1/2}$ in natural convection theory (Equation 23.12 in [32])
K_0	modified Bessel function of the second kind, order zero
K_1	modified Bessel function of the second kind, order one
L	length of the solenoid (cm)
L_c	length of a cylindrical electrode (cm)
L_e	width of a (rectangular) plate electrode (cm)
n	number of turns per unit length of solenoid coil (cm^{-1})
P	pressure (N cm^{-2})
q	charge density (C cm^{-3})
Q	rj_rB_z (J cm^{-3}) (Table 1)
r	radial position (cm)
R	radius of a thin helical coil (cm)
R_1	inner radius of the helical coil (cm)
R_2	outer radius of the helical coil (cm)
R_M	ratio defined in Equation 26
t	time (s)
t_+	cationic transference number (-)
u	$2\pi na$ (-)
v	velocity vector (m s^{-1})
v_A	Alfvén wave velocity (cm s^{-1})
x	cartesian coordinate direction (cm)
y	cartesian coordinate direction (cm)
z	cartesian coordinate direction (cm)

z_+ cationic valency (-)

Greek symbols

α densification coefficient (-)
β_1; β_2 inclination angles between the axial search point and solenoid ends (radian)
γ Levich parameter in natural convection theory, $0.48/Sc^{1/4}$ ($Sc = \nu/D$; Schmidt number)
δ_i dispersion parameter (cm)
δ_N thickness of the Nernst diffusion layer (cm)
δ_m mean thickness of the convective diffusion layer (cm)
Δ length of the dispersion layer (cm)
η dimensionless convective diffusion layer coordinate (cm); η_0 layer thickness
θ azimuthal angle (radian)
μ permeability of the electrolyte (Vs A^{-1} cm^{-1})
ν kinematic viscosity of the electrolyte (cm^2 s^{-1})
ν_+ cationic stoichiometric coefficient (dimensionless)
ρ electrolyte density (g cm^{-3})
ϕ function defined by Equation 13(a)
Φ integral defined in Equation 17
ψ function defined by Equation 3(a)
$\boldsymbol{\omega}$ vorticity vector (s^{-1})

Subscripts

x, y, z, r, θ component directions
o magnitude

Special *symbols*

$*$ superscript, denoting mean value at $\eta_0/2$
$D\xi/Dt$ substantial derivative of vector ξ, $\partial\xi/\partial t + (\xi \bullet \nabla)\xi$
∇ gradient operator
$\nabla\bullet$ divergence operator
$\nabla\times$ curl operator
∇^2 laplacian operator

1. Introduction

Electrolysis carried out under the influence of magnetic fields has provided a significant extension to the horizon of modern electrochemical science; its contributions have been summarized in various publications (e.g., [1–6]). Enhanced rates in electrodeposition, creation of specific growth patterns of electrodeposits, and specific surface conditioning are major benefits of magnetic field superposition on electric fields, the latter responsible for primary current flow.

A large majority of experimental investigations are linked to uniform magnetic fields, although earlier reports describe certain hydrodynamic phenomena generated in nonuniform fields (e.g., [7–10]). An in-depth analysis of inhomogeneous magnetic induction effects has been attempted only lately, and a recent publication [11] may be regarded as a 'precursor' to the detailed theoretical treatment offered in the current paper.

The principal objective for utilizing nonuniform magnetic fields (NMF) is the generation, locally or in the entire liquid body, of magnetohydrodynamic (MHD) turbulence, which can be a promoter of high ionic mass transport rates. In turn, electrode process rates may be enhanced at preferential local surfaces, or along the entire surface, provided that the process is essentially mass transport-controlled.

The purpose of this paper is to present an MHD-based framework for the analysis of electrolysis carried out under NMF conditions, with specific reference to certain experimental observations reported in the literature. It is hoped that it will contribute to a deeper understanding of MHD phenomena in electrolytes, and that further work in this research area will be stipulated.

2. Theory

2.1. *Magnetic field distribution in solenoids*

The classical theory of solenoidal fields [12] yields three fundamental relationships for the magnetic flux density (magnetic induction) distribution in the axial and transverse directions in a solenoid made up of n turns per unit length and radius R, carrying electric current I. If the thickness of the winding is negligible with respect to the radius of the helical coil, the magnetic flux density components can conveniently be expressed in terms of cartesian coordinates [12] as

$$B_x = 0 \tag{1a}$$

$$B_y = -n\mu I[2\pi nRK_0(2\pi nR) + K_1(2\pi nR)] \tag{1b}$$

and

$$B_z = \tfrac{1}{2}n\mu I(\cos\beta_2 - \cos\beta_1) \tag{1c}$$

in terms of modified Bessel functions; μ, the permeability of the medium is essentially that of vacuum. The angles β_1 and β_2 are defined by connecting a search point on the axis at a distance b from the solenoid centre at $z = 0$, to the opposite ends of the winding at $z = -L/2$ and $z = L/2$. If the thickness of the winding is also accounted for, the relationships

$$B_x = 0 \tag{2a}$$

$$B_y = -n\mu I\psi(u) \tag{2b}$$

and

$$B_z = \tfrac{1}{2}n\mu IF(a, b) \tag{2c}$$

replace Equation 1, with auxiliary quantities $a = (R_1 + R_2)/2; u = 2\pi na$; then

$$\psi(u) = uK_0(u) + K_1(u) \tag{3a}$$

and

$$F(a,b) = \frac{(L/2+b)}{\sqrt{a^2+(L/2+b)^2}} + \frac{(L/2-b)}{\sqrt{a^2+(L/2-b)^2}} \tag{3b}$$

provided that the geometric aspect ratio L/R is sufficiently large. In the limit, $B_y \to 0$, and $B_z \to n\mu I$, as $L/R \to \infty$. A more detailed analysis [13], not included here, provides field distributions at separate locations, that is, in the central zone and the off-centre zone along and off the axis. It also extends analysis to non-circular (e.g., rectangular) coils. The complicated computation scheme involves elliptic integrals and Legendre polynomials, but extensive tabulations [13] alleviate to some extent the burden of computation of the $\boldsymbol{B}$ field at arbitrary coordinate positions. It follows from Equation 3(a) that, if u is sufficiently large, the transverse components are negligible and the generated magnetic field is essentially axial, albeit non-uniform, along the axis.

2.2. *MHD phenomena in an electrolyte contained inside a solenoid*

In an incompressible fluid medium the fundamental Navier–Stokes equation may be expressed [14] as

$$\rho\frac{\partial \boldsymbol{v}}{\partial t} + \nabla\left(\frac{v^2}{2}\right) - \boldsymbol{v}\times(\nabla\times\boldsymbol{v}) = -\nabla P + \rho\nu\nabla^2\boldsymbol{v} + \boldsymbol{F}_{\mathbf{T}} \tag{4}$$

where

$$\nabla^2\boldsymbol{v} = \nabla(\nabla \bullet \boldsymbol{v}) - \nabla\times(\nabla\times\boldsymbol{v})$$

and $\boldsymbol{F}_{\mathbf{T}}$ is the total of all external force vectors. In combined electric/magnetic fields, an important component of the total force is $\rho\boldsymbol{E} + \boldsymbol{j}\times\boldsymbol{B}$. The first term represents conduction and the second term is known as the MHD body force density. Its expanded form

$$\boldsymbol{j}\times\boldsymbol{B} = (\nabla\times\boldsymbol{B})\times\frac{\boldsymbol{B}}{\mu} = (\boldsymbol{B}\bullet\nabla)\frac{\boldsymbol{B}}{\mu} - \frac{\nabla B^2}{2\mu} \tag{5}$$

represents magnetic stiffness, and the magnetic pressure gradient, respectively [15]. The current density vector $\boldsymbol{j}$, not to be confused with $\boldsymbol{j}_{\mathbf{s}}$ carried by the solenoid winding, is an implicit function of $\boldsymbol{B}$ in an electrolyte, if the electric field is strong enough to impose mass transport control at the electrodes. In weak electric fields it may be considered as an independent variable. The ratio of the magnitude of terms in Equation 5 to the magnitude of terms in Equation 4 expresses the relative importance of the magnetic force per unit volume of the fluid [16]. If the two quantities are equal, equipartition is achieved, where the velocity magnitude is related approximately to the magnetic flux density as

$$v_{\mathrm{A}} \approx \frac{B}{\sqrt{\rho\mu}} \tag{6}$$

known as the Alfvén wave velocity, provided that the right hand side of Equation 4 contains only the pressure gradient and the MHD body force density. In electrolytes a study of MHD-generated waves requires a more involved analysis [17]. (The indiscriminate use of the equipartition principle would predict $v_{\mathrm{A}} \approx 28$ m s^{-1} in a $B = 1$ tesla field in a common aqueous electrolyte!)

The right-hand side of Equation 5 is interpretable as the Maxwell stress gradient, and the second term, the magnetic pressure, represents an isotropic compressive stress [18]. If the magnetic induction lines are not curved, Equation 4 yields $P + B^2/2\mu = \text{constant}$ at equilibrium. The principal Maxwell stresses arising from $\boldsymbol{B}$ are composed of $B^2/2\mu$ tension along the field lines, and $B^2/2\mu$ compression in all transverse directions. Since '$\ldots \boldsymbol{j}\times\boldsymbol{B}$ forces are in general rotational and create vorticity$\ldots$' ([15], problem 4.15, p. 10), the magnetic field effect on hydrodynamic behaviour may also be traced conveniently (and often more efficiently) in terms of the vorticity relationship

$$\frac{\mathrm{D}(\boldsymbol{\omega}/\rho)}{\mathrm{D}t} - \left(\frac{\boldsymbol{\omega}}{\rho}\right)\bullet\nabla\boldsymbol{v} = \frac{1}{\rho}\nabla\times\left(\boldsymbol{j}\times\frac{\boldsymbol{B}}{\rho}\right) + \nu\nabla^2\boldsymbol{\omega} \tag{7}$$

where the vorticity vector $\boldsymbol{\omega} \equiv \nabla\times\boldsymbol{v}$ represents the angular velocity of an infinitesimal fluid element. The usefulness of a vorticity-based approach in interpreting the magnetic field effect on various electrolytic cell geometries is explored in the sequel.

2.3. *An overall view of MHD effects on electrolysis*

The interference of an externally imposed magnetic field with the velocity field in the boundary layer is manifest by the magnetic force component of $\boldsymbol{F}_{\mathbf{T}}$ in Equation 4. It then follows directly from convective diffusion theory [20, 21] that the ionic concentration distribution

$$\frac{\partial c_{\mathrm{I}}}{\partial t} + \boldsymbol{v}\bullet\nabla c_{\mathrm{I}} = \nabla\bullet(D_{\mathrm{I}}\nabla C_{\mathrm{I}}) \tag{8}$$

can undergo a significant modification due to the magnetically modified velocity field. Equation 8 applies in a strict sense only to a dilute binary electrolyte in the presence of a supporting electrolyte of sufficient concentration, but the treatment required for concentrated solutions is well beyond the scope of this paper, inasmuch as the usual complications encountered via the theory of irreversible thermodynamics [22, 23] become even more severe. If migration due to charge transfer cannot be neglected, the more general form of Equation 8, expressed as [24]

$$\frac{\partial c}{\partial t} + \boldsymbol{v}\bullet\nabla c = \nabla\bullet(D\nabla c) - \frac{(\boldsymbol{j}\bullet\nabla_{t+})}{z_+ v_+ F} \tag{9}$$

indicates the necessity of knowing the diffusivity gradient due to the concentration field (and possibly to the magnetic field, but to a much smaller extent), as well as the transference number gradient. In consequence, a straightforward solution of Equation 8 or 9 is not feasible (this fact remains a fundamental challenge for the theory of magnetoelectrolysis).

An alternative approach to the analysis of global magnetic field effects (i.e., at current flows where secondary interactions due to paramagnetism etc. can be neglected) entails the study of vorticity formation. The effectiveness of this approach, justified inside a solenoid due to the existence of field inhomogeneity, was demonstrated earlier in the absence of a solenoid [25], and has recently been discussed at some length [11] for certain configurations.

2.4. *Vorticity analysis in magnetoelectrolysis carried out inside a solenoid*

2.4.1. *Cylindrical cells in helical solenoids*

In this configuration a cylindrical cell with an appropriate electrolyte occupying the space between two concentric cylindrical electrodes is surrounded by helical coils which generate the magnetic field. Neglecting secondary effects, the MHD characteristics assembled in Table 1 provide a reasonably accurate description of the forcing elements in action. Under such circumstances, the approximating vorticity field equations can be written as

$$\frac{\partial \omega_r}{\partial t} - \frac{\partial (v_\theta \omega_r)}{\partial z} = \frac{1}{\rho r}\frac{\partial Q}{\partial z} \tag{10a}$$

$$\frac{\partial \omega_\theta}{\partial t} = 0 \tag{10b}$$

$$\frac{\partial \omega_z}{\partial t} - \frac{\partial (v_\theta \omega_r)}{\partial r} = -\frac{1}{\rho r}\frac{\partial Q}{\partial r} \tag{10c}$$

if viscous effects are assumed to be small with respect to the magnetic field contribution to vorticity. Further manipulations are shown in Section 3, in applying the theory to specific experimental cells.

Table 1. MHD characteristics of cylindrical electrolytic cells in helical solenoids

Characteristic	Equation
Current	$\boldsymbol{j} = \boldsymbol{e}_r j_r$
Magnetic flux density	$\boldsymbol{B} = \boldsymbol{e}_r B_r + \boldsymbol{e}_z B_z$
Velocity	$\boldsymbol{v} = \boldsymbol{e}_\theta v_\theta$
Vorticity	$\omega = \boldsymbol{e}_r \omega_r + \boldsymbol{e}_z \omega_z$
MHD body force density	$-\boldsymbol{e}_\theta j_r B_z$
Vortex analysis components	$\nabla \times (\boldsymbol{j} \times \boldsymbol{B}) = \frac{1}{r}\left[\boldsymbol{e}_r \frac{\partial Q}{\partial z} - e_z \frac{\partial Q}{\partial r}\right]$
	$\boldsymbol{v} \times \boldsymbol{\omega} = \boldsymbol{e}_r (v_\theta \omega_z) - \boldsymbol{e}_z (v_\theta \omega_r)$
	$\nabla \times (\boldsymbol{v} \times \boldsymbol{\omega}) = -\boldsymbol{e}_r \frac{\partial (v_\theta \omega_r)}{r \partial \theta}$
	$+ \boldsymbol{e}_\theta \left[\frac{\partial (v_\theta \omega_z)}{\partial z} + \frac{\partial (v_\theta \omega_r)}{\partial r}\right] - \boldsymbol{e}_z \frac{\partial (v_\theta \omega_z)}{r \partial \theta}$

2.4.2. *Rectangular cells in helical solenoids*

The preceding analysis can readily be adapted to rectangular cells, employing cartesian coordinates in the case of plate electrodes. If $L/R \gg 1$, the $\boldsymbol{B}$ distribution is given essentially by Equations 2(c) and 3(b), but the current distribution is no longer purely radial, and the velocity field is at least two-dimensional. Such cell/solenoid configurations are less practical than the configuration discussed in Section 2.4.3.

2.4.3. *Rectangular cells in rectangular solenoids*

As illustrated in Section 3, such experimental configurations have been presented in the literature. The major challenge here is the determination of the magnetic flux density distribution inside the cell, based on certain models approximating rectangular coils. The 'superposition of building block' principle [26] requires involved computations, but if the coil is sufficiently long, end effects can be neglected, and the rectangular coil may be represented by the superposition of four finite rectangular bars [26]. The finite-length coil case requires more complex calculations, but graphs and tabulations (e.g., [27]) reduce somewhat the computational burden.

In rectangular-shaped solenoids an arbitrary $\boldsymbol{B}$ field distribution can also be created by nonuniform coil-winding techniques [10], but the field distribution has to be measured experimentally. Such configurations are excellent for creating extremely inhomogeneous magnetic fields which, in turn, produce strongly nonlinear vorticity effects, albeit at the expense of manageable mathematical description.

3. Application to experimental magnetoelectrolytic cells operating in solenoids

3.1. *Dissolution/deposition of copper in a cylindrical cell inside a helical solenoid*

The cell employed by Sundermann [28, 29] contained an outer copper cylinder with a 5.0 cm active diameter, and a 0.9 cm diameter solid inner copper rod; both electrodes had an active length of 4.7 cm. The cell contained aqueous $CuSO_4$ solutions, and was positioned in the central region of a 40 cm long, 8.8 cm diameter cylindrical solenoid. The magnetic field was generated by a four layers deep 18 AWG magnet wire winding with 1424 total turns. The magnitude of the modified Bessel functions in Equation 3(a) being about 10^{-450} ($a = 4.61$ cm; $n = 35.6$ cm^{-1}), the field is fully axial with a variation of $F(a, b)$ from about 1 ($b = L/2$) to about 1.95 ($b = 0$) inside the cell. Due to the high conductivity of copper, the axial variation of the radial current may be neglected. Then, under galvanostatic control, $j_r = I/2\pi L_c r$ is a simple hyperbolic function of radial position. In consequence, the vorticity field is given by

$$\frac{\partial \omega_r}{\partial t} - v_\theta \frac{\partial \omega_r}{\partial z} \approx \left(\frac{k_1}{r}\right)\frac{\partial B_z}{\partial z} \tag{11a}$$

and

$$\frac{\partial \omega_z}{\partial t} - v_\theta \frac{\partial \omega_r}{\partial r} - \omega_r \frac{\partial v_\theta}{\partial r} \approx \left(\frac{k_1}{r}\right) \frac{\partial B_z}{\partial r} \approx 0 \qquad (11b)$$

if natural convection is neglected on account of the (anticipated) intensity of induced azimuthal motion. Under steady-state conditions, the azimuthal velocity field may be approximated by the simplified Navier–Stokes equation

$$r^2 \frac{\partial^2 v_\theta}{\partial r^2} + r \frac{\partial v_\theta}{\partial r} - v_\theta = -k_2 B_z r \qquad (12)$$

whose solution may be written in the dimensionless form

$$\left(\frac{\pi \mu}{I B_z}\right) v_\theta = \phi(r) \qquad (13a)$$

where ϕ is a dimensionless velocity function of the radial position, defined as

$$\phi(r) \equiv \frac{r}{2L_c} \ln\left(\frac{R}{r}\right) - \left[r_0^2 \ln \frac{R/r_0}{2L_c(R^2 - r_0^2)}\right]\left(\frac{R^2 - r^2}{r}\right) \qquad (13b)$$

As shown in Figure 1, the velocity reaches a local maximum at the radial position of about 1.25 cm, at which the gradient $\psi(r) \equiv 2L_c \mathrm{d}\phi/\mathrm{d}r$, illustrated in Figure 2, becomes locally zero. The graphs indicate that vorticity effects are largest at the electrode–electrolyte interfaces: at the inner electrode, $\mathrm{d}v_\theta/\mathrm{d}r$ is about 3.16 s^{-1} and at the outer electrode, -1.27 s^{-1}, for 1 A current and 1 mT magnetic flux density.

3.2. *Dissolution/deposition of copper in a multiple electrode rectangular cell inside a rectangular solenoid*

An experimental cell [30] described earlier (Figure 1 in [31]) contained five 15 cm wide, 25 cm long and 0.4 cm thick copper plates connected in an alternating C—A—C—A—C (C cathode; A anode) pattern. The cell was sealed in the interior space of a 26 cm × 26 cm × 10 cm PVC container which was fully enclosed in a jacket with a 960 turn AWG 14 copper wire coil, consisting of 12 layers, wound on its outside wall. The electrolyte

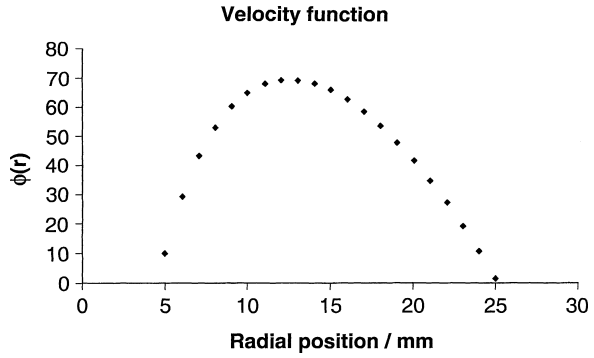

Fig. 1. Velocity function $\phi(r)$ as a function of radial position in the cell of Section 3.1.

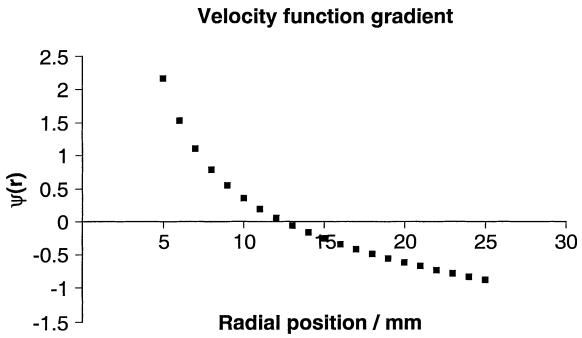

Fig. 2. Velocity function $\Phi(r)$ as a function of radial position in the cell of Section 3.1.

solutions were aqueous $CuSO_4$ dissolved in sulphuric acid of high concentration (1.50–1.62 mol dm^{-3}). The active electrode area was kept at 700–800 cm^2 per electrode face. The essentially axial mean magnetic flux density varied between 4.0 (residual strength) and 785 mT. The transverse field components were of a 10^{-4}–10^{-6} order of magnitude, relative to B_z in the near corner areas, and completely negligible elsewhere in the cell. In this configuration, natural convection at the cathode plates cannot be *a priori* neglected, and the vorticity analysis below considers a symbiotic effect of magnetic field and convective buoyancy forces.

The rectangular coordinates are x normal to the electrode plates, y parallel to the electrode plates and z axial. The origin of the coordinate system is placed at one of the lower edges of a cathode plate. To keep mathematical encumbrance at a modest level, it is postulated that classical convective diffusion theory applied to natural convection at vertical plates can be applied without structural modifications. The following simplifications are introduced at this stage: (i) the induced electric currents are negligible because of the low magnetic Reynolds number, hence $O[j_x] \gg O[j_y; j_z]$; (ii) inside the boundary layer $O[\partial\rho/\partial z]$ and $O[\partial\rho/\partial x]$ are much larger than $O[\partial\rho/\partial y]$, following the conventional postulation of y symmetry in natural convection theory. Hence, the right-hand side of Equation 7 may be simplified to the form of

$$\frac{1}{\rho}\nabla\times(\boldsymbol{j}\times\boldsymbol{B}) \approx -\boldsymbol{e}_x\left[\frac{\partial j_x B_z}{\rho \partial z} + \left(\frac{j_x B_z}{\rho^2}\right)\frac{\partial \rho}{\partial z}\right] + \boldsymbol{e}_z\left[\frac{\partial j_x B_z}{\rho \partial x} + \left(\frac{j_x B_z}{\rho^2}\right)\frac{\partial \rho}{\partial x}\right] \qquad (14)$$

It then follows that only ω_x and ω_z are influenced by the magnetic field, and they can be analysed separately.

(a) *Analysis of* ω_x. Since the magnitude of the gravity force density in an aqueous electrolyte with density about 1 kg dm^{-3} is approximately 9.81 N dm^{-3}, a current density of 981 A dm^{-2} would be necessary to generate an MHD body force density of 9.81 N dm^{-3} at a magnetic flux density of 100 mT. Experimentally observed current densities [30, 31] ranging from 0.23 to 0.38 A dm^{-2} are about three orders of magnitude

smaller, suggesting that under such conditions magnetic fields are not likely to interfere appreciably with the structure of the boundary layer. In consequence, it may be assumed that $\partial\rho/\partial z$ is the predominant density gradient (except right on the interface). Similarly, inside the solenoid, $\partial B/\partial z$ is predominant, and v_x as well as ω_x possess y symmetry. As shown in a previous study [25], the ω_x derivatives are much larger than the v_x derivatives, and $\partial(\omega_x/\rho)/\partial z \gg \partial(\omega_x/\rho)/\partial x$. Thus, at steady state conditions,

$$v_z \frac{\partial(\omega_x/\rho)}{\partial z} = -\left(\frac{j_x}{\rho^2}\right)\frac{\partial B_z}{\partial z} - \left(\frac{B_z}{\rho^2}\right)\frac{\partial j_x}{\partial z} - \left(\frac{j_x B_z}{\rho^3}\right)\frac{\partial \rho}{\partial z} \tag{15}$$

Since the imposed current is essentially independent of the z coordinate, the second term on the right hand side of Equation 15 is negligible with respect to the first term, yielding

$$\frac{v_z}{\rho}\frac{\mathrm{d}\omega_x}{\mathrm{d}z} - \frac{v_z\omega_x}{\rho^2}\frac{\mathrm{d}\rho}{\mathrm{d}z} = -\frac{j_x}{\rho^2}\frac{\mathrm{d}B_z}{\mathrm{d}z} - \frac{j_x B_z}{\rho^3}\frac{\mathrm{d}\rho}{dz} \tag{16}$$

which may be integrated by virtue of the integrating factor $\exp[\rho(1-\ln\rho)]$, following closely an earlier development (Appendix of [25]). The integrated form may be written as

$$\omega_x^* = \left(\frac{j_x}{\rho^* K}\right)[\Phi(h) - \Phi(z)] + \frac{j_x B_z \alpha(1-c^*)}{2\rho^0 K(1-\alpha c^*)} \times (h^{-1/2} - z^{-1/2}) \tag{17}$$

where $\Phi(z) \equiv \int(\partial B_z/\partial z)z^{-1/2}\,\mathrm{d}z$. The first term in Equation 17 accounts for the nonuniformity of the magnetic field, whereas the second term pertains to natural convection in a uniform magnetic field. The * superscript signifies that the appropriate quantities are estimated at one-half of the dimensionless convective diffusion layer thickness, that is, at $\eta^* = \eta_0/2$, according to natural convection theory (Equation 23.23 of [32]). Note that the second term in Equation 17 corresponds to the right hand side of Equation A.6 in [25], except for the erroneous squaring of the $(1-\alpha c^*)$ term in the latter.

(b) *Analysis of* ω_z. Figure 3(a) illustrates the electric current path in the cell. At each electrode there is a sudden change in the direction of the electric current which, in itself, is a function of the distance measured from the lower edge of the electrode (in pure natural convection, e.g., j_x is proportional to $z^{-1/4}$).

A charge balance on the shell volume in Figure 3(b), that is,

$$bL_e(\mathrm{d}z)\frac{\partial q}{\partial t} = bL_e j_z - bL_e\left[j_z + \left(\frac{\partial j_z}{\partial z}\right)\mathrm{d}z\right] + L_e(\mathrm{d}z)j_x \tag{18}$$

yields the steady state current distribution $\partial j_z/\partial z = j_x/b$ in the electrodes. The variation of j_x can be approximated by the periodic waveform shown in Figure 3(c),

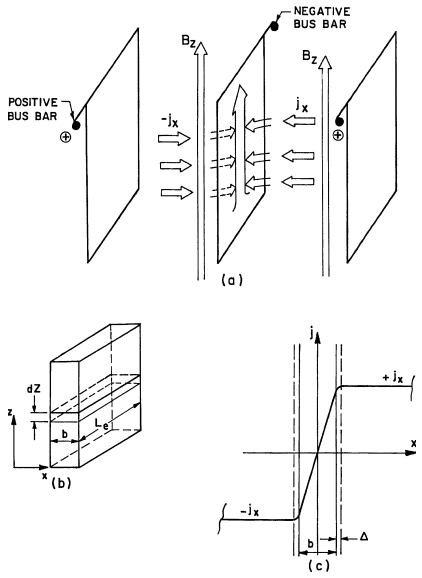

Fig. 3. Change in the direction of the current flow through the electrolyte solution at the electrodes in the cell of Section 3.2. (a) Schematic view of a cathode; (b) illustration for charge flow balance in a cathode; (c) approximation to the current flow to the cathode: pattern of the periodic functional form.

where Δ represents the length of a 'dispersion' region in the immediate neighbourhood of the electrodes. Within this region the change in current direction is the result of a gradual continuous process which is more realistic than a sharp (mathematically inspired) discontinuity. Since $\Delta \ll b$, the function shown in Figure 3(c) may be represented by the Fourier series [33]

$$j_x = \frac{4bj_0}{\pi^2(b/2+\Delta)}\sum_{n=0}^{\infty} f$$
$$f(n,x) \equiv \sin\left[\frac{(2n+1)\pi(b/2+\Delta)}{b}\right] \times \sin\left[(2n+1)\frac{\pi x}{b}\right] \times \frac{1}{2n+1} \tag{19}$$

Thus, for $0 < x < b/2+\Delta$, j_x possesses a nonzero x derivative, and if $j_x\partial B_z/\partial x$ is rather small with respect to $B_z\partial j_x/\partial x$, arguments presented above lead to the steady state equation

$$v_x\frac{\partial(\omega_z/\rho)}{\partial x} \approx \frac{B_z}{\rho^2}\frac{\partial j_x}{\partial x}; \quad \frac{b}{2} \leqslant x \leqslant \frac{b}{2}+\Delta \tag{20a}$$

with a convergent [34–36] current density gradient

$$\frac{\partial j_x}{\partial x} = \frac{4j_0}{\pi(b/2+\Delta)}\sum_{n=0}^{\infty} f(x,n) \tag{20b}$$

Since

$$\frac{\partial j_x}{\partial x} < \frac{4j_0}{\pi(b/2+\Delta)}\sum_{n=0}^{\infty}\cos\left[(2n+1)\left(\frac{\pi x}{b}\right)\right] \times \frac{1}{2n+1} \tag{20c}$$

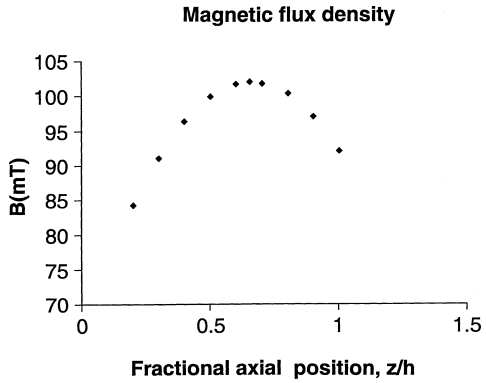

Fig. 4. A typical variation of the measured axial magnetic flux density with axial position in a multiple electrode cell [32, 33] containing 0.08 mol dm^{-3} cupric sulfate and 1.60 mol dm^{-3} sulfuric acid. $h = 15.24$ cm; $d = 25.4$ cm.

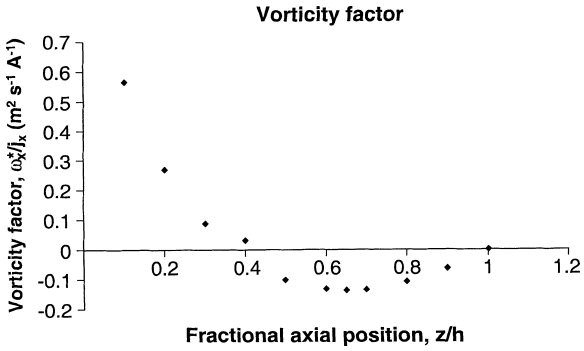

Fig. 5. Variation of the x-directed vortex component (Equation 17) associated with conditions indicated for Figure 4.

follows immediately, and since the limit of the infinite series in Equation 20(c) is given by the closed form $\ln|\mathrm{cotan}(\pi x/2b)|$, further simplifications yield the inequality

$$\frac{\partial j_x}{\partial x} < \frac{2j_0}{\pi(b/2+\Delta)}\ln\left(\frac{2b}{\pi x}\right); \quad x \ll b \tag{21}$$

The final step before integrating Equation 20(a) is the estimation of v_x. Since Δ is very small, an approximate value, averaged over the electrode height may be obtained from the truncated form of the expansion given by Levich [32]:

$$v_x \approx -\left(\frac{2\gamma\nu}{h^{3/4}}\right)\left(\frac{g\alpha}{4\nu^2}\right)^{3/4}x^2 \tag{22}$$

Substituting Equations 21 and 22 into Equation 20(a), and integrating from x to $b/2+\Delta$, the expression

$$\omega_z \leqslant \left[\frac{j_0 B_z h^{3/4}}{\pi(b/2+\Delta)^2\gamma\nu(g\alpha/4\nu^2)^{3/4}}\right]\left\{\left[\ln\frac{2b}{\pi(b/2+\Delta)}\right] - \left[\frac{(b/2+\Delta)}{x}\ln\frac{2b}{\pi x}\right] - \left[1-\frac{(b/2+\Delta)}{x}\right]\right\} \tag{23}$$

is finally obtained, within a distance δ_i measured from the electrode surface. In summary, the vorticity distribution

$$\omega = \boldsymbol{e}_x\left(\frac{\partial v_z}{\partial y}-\frac{\partial v_y}{\partial z}\right)+\boldsymbol{e}_z\left(\frac{\partial v_y}{\partial x}-\frac{\partial v_x}{\partial y}\right) \tag{24}$$

indicates the existence of a three-dimensional velocity field, with component directions being opposite on the two sides of the electrodes. The resulting motion is a closed-loop vortex around the electrodes, observed also experimentally [31]. A typical variation of the magnetic flux density (Figure 4) and one vorticity component (Figure 5) along the axis indicate the coincidence of local extrema in these quantities. The estimation of the z directional vorticity component is more involved due to the *a priori* indeterminacy of the dispersion length, but it is to be noted that it takes up a very small fraction of the convective diffusion layer thickness, inasmuch as the change in direction of the current flow near an electrode surface must begin at a very small distance from it. Under the experimental conditions of Figure 4, Equation 23 may be written as

$$\omega_z = -0.007\,493\left(\frac{j_x B_z}{\delta_i^2}\right)\left[\ln\frac{0.016\,17}{\delta_i} - \left(\frac{\delta_i}{x}\right)\ln\frac{0.016\,17}{x} - \left(1-\frac{\delta_i}{x}\right)\right]\ \mathrm{s}^{-1} \tag{25}$$

On the basis of convective diffusion theory applied to natural convection at vertical plate electrodes [32, 37], $\Delta = 10^{-4}$ cm is assumed, then $\delta_i \approx 0.02$ cm is a reasonable estimate of the dispersion parameter δ_i. Thus, at $x = (b+\Delta)/2 \approx 0.02$ cm, the vorticity component $\omega_z < 2\times10^8 j_0 B_z\ \mathrm{s}^{-1}$. Hence, at the highest magnetic flux density of 785 mT, the magnitude of ω_z is less than about $1.6\times10^4\, j_0\ \mathrm{s}^{-1}$, its direction being positive (counterclockwise) on one side of the electrode, and negative (clockwise) on its other side. Thus, a strong vortex is forming a 'tight' closed loop around an electrode within distance δ_i. The actual magnitude of ω_z is most likely much smaller than its hereby estimated upper bound, but even if it were three or four orders of magnitude smaller, it would be still much larger than the magnitude of ω_x within $0 < x < \delta_i$. In the large remainder of the convective diffusion layer (i.e., $\Delta < x < \delta_N$), the vorticity effect is due essentially to the nonuniformity of the magnetic field. Closed-loop vortex motion was, indeed observed [31] by means of light particles travelling on the electrolyte surface around the electrodes, whose speed and curvature indicates a strong dispersion of the generated vorticity effect into the electrolyte bulk (i.e., several millimetre from the electrode).

4. Implications for the design of magnetoelectrolytic cells operating inside solenoids

The prime result of a vorticity-based analysis is that cells placed into a solenoid zone with significant magnetic

field asymmetry can be expected to undergo the highest possible turbulence/vortex generation. This is a major avenue of magnetically enhanced mass transport rates. Such 'optimal' regions can, in effect, be found even in large geometric aspect-ratio solenoids, as demonstrated below, in the case of medium diameter helical solenoids with a small number of turns. As indicated by Equation 3(a), if u is small, the magnitude of the $\psi(u)/F(a, b)$ ratio may remain larger than zero; even at the relatively large value of $u = 6$, $\psi(u) = 0.008\,81$ and at $u = 9$, $\psi(u) = 0.000\,511$. Table 2 illustrates the existence of relatively large local (B_y/B_z) gradients in a 'border' zone taking up approximately 1% of the total solenoidal length. The transverse field strength becomes, in fact, larger in magnitude than the axial field strength within this zone. It is worth noting, however, that if the number of coil turns were large, the degree of field inhomogeneity would be smaller, if existing at all, and the solenoid field would be essentially axial with a small (albeit nonzero) $\partial B_z/\partial z$ gradient (e.g., if $n = 5\,\mathrm{cm}^{-1}$, and $a = 2$ cm, $\psi(u) \approx 5 \times 10^{-27}$ and $B_y \approx 0$, in accordance with Equation 3(a)). Magnetoelectrolysis carried out inside rectangular solenoids on a pilot–plant scale [10, 38] suggest practical applications in the electroplating, electrowinning and electrorefining of aqueous metal-ion solutions. As shown in these references, electric current to such cells could be applied via bus bar or pipe sections joined by means of elbow pieces in such a manner that the bars form a rectangular coil consisting of a few turns around the electrolytic cell. The solenoid can be excited by the d.c. current required for electrolysis, and relatively large currents can be passed if cooling water is flown through the pipe sections to minimize temperature rise in them. These are important engineering aspects, since the additional modest ohmic voltage drop costs encountered in operating the solenoid would be offset by increased profits from higher production rates. In the case of new installations, smaller tank construction costs would be realisable, inasmuch as cell volumes at a fixed current level could be smaller than in the absence of a magnetic field. It is also well known (e.g., [1–3]) that higher current densities in magnetoelectrolysis do not cause electrode surface deterioration under proper operating conditions, hence current densities well above current industrial limits can be envisaged.

Table 2. Magnetic field characteristics in a (hypothetical) medium diameter solenoid with a small number of coil turns
$L = 1$ m; $n = 10\ \mathrm{m}^{-1}$; $a = 2$ cm; $\psi(u) = 0.7684$.

b /cm	$F(a, b)$ /(dimensionless)	$\lvert B_y/B_z\rvert$ /(dimensionless)	$B^2/2\mu$ /μN m^{-2}
0	1.9984	0.769	99.82
5.0	1.9983	0.769	99.82
10.0	1.9982	0.769	99.81
20.0	1.9974	0.769	99.76
30.0	1.9947	0.770	99.59
40.0	1.9803	0.776	98.69
45.0	1.9283	0.797	95.50
46.0	1.8942	0.8113	93.45
47.0	1.8318	0.8389	89.80
48.0	1.7169	0.9003	82.86
49.0	1.4470	1.0620	69.98
49.5	1.2423	1.2370	61.33
49.6	1.1959	1.2850	59.56
49.7	1.1481	1.3385	57.80
49.8	1.0993	1.3980	56.07
49.9	1.0497	1.4640	54.40
50.0	0.998	1.5370	53.00

5. Implications for electrochemical mass transport

The major implication for electrochemical mass transport stems from the beneficial effect of magnetic field imposition on turbulence generated at the electrode–electrolyte interface; the convective component of convective diffusion may thus become the dominant driving force for ion transport. As a result, the mean thickness δ_m of the convective–diffusion boundary layer is reduced and, in consequence, the ionic mass transport coefficient k_m is increased. Since the effect of magnetic fields on diffusivity is extremely small [1], enhancement in specific mass transport rates is directly linked to a decrease in δ_m, under full mass transport control. Under such conditions, the mass transport coefficient in a magnetic field may be estimated from the relationship

$$R_M \equiv \frac{(k_m)_B}{(k_m)_{B=0}} = \frac{i_B}{i_{B=0}} \tag{26}$$

at a sufficiently cathodic fixed potential to ensure mass transport control.

If turbulence is sufficiently strong, certain local sections of the boundary layer may be extremely thin, while other sections may be relatively thick. Heavy deposits may then alternate with essentially deposition-free domains on the cathode surface [10, 38]. Under such conditions, quantitative estimation of the turbulence effect cannot be made reliably.

At current levels below the limiting plateau, where mass transport and charge transport share control of the ion transport process, system complexity [39] thwarts the application of simple relationships. In a first approximation, the effect of charge transfer on current density in magnetoelectrolysis may be accounted for, at least in principle, by the modified Equation 7 in [40]:

$$|i_B| = zFD\frac{(c_\infty - c_e)}{\delta_m(1 - t_+)} \tag{27}$$

if the Nernst layer thickness is replaced by the mean boundary layer thickness. However, the simultaneous effect of magnetic fields on boundary layer thickness and cationic transport number has to be known. To the author's knowledge, no such quantitative relationships exist at present in the literature.

6. Final remarks

While vorticity generation due to interaction of inhomogeneous magnetic fields with an electric field is the primary cause of ionic flow enhancement (in addition to enhancement produced in homogeneous fields), the opposite phenomenon: vorticity suppression, can also be observed under certain conditions. A specific instance, where the $\nabla\times(\boldsymbol{j}\times\boldsymbol{B})$ term opposes vorticity in a flow cell exposed to a uniform transverse magnetic field is shown [41] to possess a characteristic vorticity relaxation time $\rho/\sigma B^2$. In magnetoelectrolysis, carried out inside a solenoid, special advantage can be taken of the well-known fact in MHD theory, that a '...mean motion and/or turbulence of the electromagnetic quantities must occur in addition to the fluid turbulence...' [42], so that $\boldsymbol{j}\times\boldsymbol{B}$ is rotational and creates vorticity. A case in point, turbulent flow propagation in the wake of local vortex creation has been documented via a laser-based visualization technique [43].

Acknowledgement

The author is grateful to the Natural Sciences and Engineering Research Council of Canada (NSERC) for support of his research in this field.

References

1. T.Z. Fahidy, *J. Appl. Electrochem.* **13** (1983) 553.
2. R.A. Tacken and L.J.J. Janssen, *J. Appl. Electrochem.* **25** (1995) 1.
3. T.Z. Fahidy, 'The Effect of Magnetic Fields on Electrochemical Processes', 'Modern Aspects of Electrochemistry', **32** (Kluwer Academic/Plenum Publishers, New York, 1999), p. 333.
4. T.Z. Fahidy, 'Characteristics of surfaces produced via magneto-electrolytic deposition', *Progre. Surf. Sci.* **68** (2001) 155.
5. Proc. Third Meeting, International Symposium on 'New Magneto – Science' '99, 24–26 Nov. 24 1999, Omiya, Japan (National Research Laboratory for Magnetic Science, Japan Science and Technology Corporation, Saitama, Japan).
6. Proc. Fourth Meeting, Symposium on 'New Magneto – Science' 2000, 13–15 Nov. 2000, Omiya, Japan (National Research Laboratory for Magnetic Science, Japan Science and Technology Corporation, Saitama, Japan).
7. S. Mohanta and T.Z. Fahidy, *Electrochim. Acta* **21** (1976) 149.
8. S. Mohanta and T.Z. Fahidy, *J. Appl. Electrochem.* **6** (1976) 211.
9. S. Mohanta and T.Z. Fahidy, *J. Appl. Electrochem.* **8** (1978) 5.
10. M.I. Ismail and T.Z. Fahidy, *Can. J. Chem. Eng.* **57** (1979) 734.
11. T.Z. Fahidy, 'MHD aspects in solenoidal magnetic fields', *Fourth International PAMIR Conference on* 'Magnetohydrodynamics at Dawn of Third Millenium', 18–22 Sept. 2000, Giens, France (LEGI, Grenoble, France) **1**, p. 351.
12. W.R. Smythe, 'Static and Dynamic Electricity', (McGraw-Hill, New York, 1968), chapter VII.
13. D.B. Montgomery, 'Solenoid Magnet Design' (Wiley-Interscience, New York, 1969).
14. W.F. Hughes and E.W. Gaylord, 'Basic Equations of Engineering Science' (McGraw-Hill, New York, 1964), chapter 3.
15. J.A. Shercliff, 'A Textbook of Magnetohydrodynamics', (Pergamon Press, Oxford, 1965), section 4.1.
16. W.M. Elsasser, 'Some dimensional aspects of hydromagnetic phenomena', 'Magnetohydrodynamics – A Symposium' (Stanford University Press, 1957), p. 16.
17. T.Z. Fahidy, *Electrochim. Acta* **21** (1976) 21.
18. J.A. Shercliff, *op. cit.* [15], section 4.2.
19. J.I. Ingraham, 'Handbook of Physics', (McGraw-Hill, New York, 2nd edn, 1958), Chapter 11, section 4.2.
20. V.G. Levich, 'Physicochemical Hydrodynamics', (Prentice Hall, Englewood Cliffs, NJ, 1962), chapter II.
21. J.S. Newman, 'Electrochemical Systems', (Prentice Hall, Englewood Cliffs, NJ, 2nd edn, 1991), chapter 11.
22. J.S. Newman, *op. cit.* [21] chapter 12.
23. R. Haase, 'Thermodynamics of Irreversible Processes', (Dover, New York, 1969), section 4–34.
24. J.S. Newman, *op. cit.* [21], section 72.
25. T.Z. Fahidy, *Electrochim. Acta* **18** (1973) 607.
26. D.B. Montgomery, *op. cit.* [13], section 8.7.1.
27. D.B. Montgomery, *op. cit.* [13], section 8.7.3.
28. R. Sundermann, 'The Generation of Electrolyte Flow by Alternating Electric and Magnetic Fields', MA Sc thesis, University of Waterloo, Canada (1974).
29. R. Sundermann and T.Z. Fahidy, *J. Appl. Electrochem.* **8** (1978) 265.
30. S. Mohanta, 'Some Aspects of Magnetoelectrolysis', PhD thesis, University of Waterloo, Canada (1974).
31. S. Mohanta and T.Z. Fahidy, *J. Appl. Electrochem.* **8** (1978) 265.
32. V.G. Levich, *op. cit.* [20], section 23.
33. K. Rektorys, 'Survey of Applicable Mathematics' (Iliffe, London, 1969), section 16.3.
34. G.P. Tolstov, 'Fourier Series'. (Dover, New York, 1976), chapter 5, sections 9, 10.
35. W. Kaplan, 'Advanced Calculus' (Addison-Wesley, Reading, MA 1952), sections 6–14, 7–11.
36. H.S. Carslaw, 'Introduction to the Theory of Fourier Series and Integrals', (Dover, New York, 1930), section 109.
37. J.S. Newman, *op. cit.* [21], chapter 17.
38. M.I. Ismail and T.Z. Fahidy, *Can. J. Chem. Eng.* **58** (1980) 505.
39. J.S. Newman, *op. cit.* [21], chapter 19.
40. G. Milazzo, 'Electrochimie 1', (Dunod, Paris, 1969), chapter IV, section 5.
41. J.A. Shercliff, *op. cit.* [15], section 4.13.
42. J.A. Shercliff, *op. cit.* [15], example 4.15, p.109.
43. Z.H. Gu and T.Z. Fahidy, *Intern. J. Engrg. Fluid Mech.* **1** (1988) 1.